Exchange splitting of *sp*-like surface states on Ni(001)

K. Starke,* K. Ertl, and V. Dose
Max-Planck-Institut für Plasmaphysik–EURATOM Association, D-8046 Garching bei München, Federal Republic of Germany
(Received 16 October 1991)

Spin-resolved inverse photoemission is employed to investigate crystal-induced and image-potential surface states on Ni(001). The observed value of the spin splitting for the crystal-induced state at $\bar{X}$ is 180±60 meV and there is experimental evidence of a nonvanishing exchange splitting of the image-potential state at $\bar{\Gamma}$. These data are consistently described within the framework of a multiple-reflection model for surface states if the upper band-gap boundaries are assumed to be exchange split by 200 meV at $\bar{\Gamma}$ and 230 meV at $\bar{X}$. For $\bar{\Gamma}$, this splitting was confirmed experimentally by spin-resolved target-current spectroscopy.

I. INTRODUCTION

Electronic surface states on ferromagnetic samples are of particular interest in surface magnetism: They serve as an indicator of magnetic properties of the uppermost atomic layer of a surface. Besides the electronic structure, the magnetic properties of the surface layer, such as exchange coupling and magnetization, can also widely differ from those of the underlying bulk. For nickel surfaces even the existence of magnetically "dead" atomic layers has been discussed.[1–3] Today, however, it is generally agreed that the top atomic layers of Ni surfaces are magnetically active.[4–9] For Ni(110) this was directly demonstrated by the large exchange splitting of surface states.[7,8]

sp-like surface states appear in Shockley-inverted gaps of the bulk band structure. Comprehensive data on the dispersion of empty *sp*-like surface bands on low-index fcc surfaces have been obtained by inverse photoemission (IPE), making it possible to discuss general trends.[10] Similarly, photoemission revealed a considerable number of occupied surface bands.[11,12] *sp*-like empty states are conveniently classified as either crystal-induced states or image-potential states.[13] Crystal-induced states can be regarded as a modification of bulk bands at the surface and have a maximum in their probability distribution in the top atomic layer. Image-potential states are a consequence of the $(1/4z)$ form of the surface-barrier potential on approaching the vacuum energy E_V. These unoccupied gap states form a Rydberg-like series spanning about 1 eV below E_V. Their wave functions, by contrast, peak a few Å in front of a crystal, thus having very little overlap with bulk bands.

Because of the widely different overlap with bulk bands, the exchange splitting is expected to be *small or negligible* for image-potential states but *considerable* for crystal-induced states. This qualitative picture has been confirmed in a multiple-reflection model[13] calculation by Borstel and Thörner.[14] Furthermore, they showed that a spin-dependent energy position of the gap edges already leads to non vanishing values for the splitting of surface states. Accordingly, for a quantitative understanding of the exchange splitting of surface states in a given gap it is essential to know the size of the bulk band splitting at the critical points which define the gap.

Only a few experiments on the exchange splitting of *sp*-like surface states have been reported so far. For a crystal-induced state on Ni(110) at $\bar{X}$, Donath *et al.*[8] observed a splitting of 170 meV. This is surprisingly large for a state located about 6 eV above the "magnetic" Ni *d* bands. No experimental values exist for the exchange splitting of image-potential states. From IPE[15] and two-photon photoemission[16] it is well known that image-potential states can be detected as well-resolved peaks only in band gaps in the region around $\bar{\Gamma}$ [center of the surface Brillouin zone (SBZ)]. Hence Fe(110), Co(0001), Ni(001), and Ni(111) constitute promising candidates for measuring the exchange splitting of image-potential states, rather than Ni(110), in which such states appear only as weak shoulders in gaps at the SBZ boundaries.[8,15] In an early spin-revolved IPE study of Fe(110) (Ref. 17) the electron beam was longitudinally polarized so that no magnetic information could be obtained at $\bar{\Gamma}$. In an investigation of Ni(001) by Klebanoff *et al.*[18] also using spin-resolved IPE even the detection of significant spin effects in bulk transitions was hindered by closure domains.[19,20] Today there are just upper bounds for a possible splitting of image-potential states at $\bar{\Gamma}$: 40 meV for Ni(111), as derived from ordinary (non-spin-resolved) two-photon photoemission,[21] and 0.1 eV for Fe(110) and Co(0001), as recently estimated from spin-integrated IPE data.[22] Altogether, the conclusive experimental verification of the exchange splitting of image-potential surface states remains a challenging task.

In the present paper we report on the exchange splitting of surface states on Ni(001). Their spin dependence is analyzed by spin-resolved IPE. Compared with an earlier spin-averaged IPE study by Goldmann *et al.*,[15] the measurement of the two-dimensional energy dispersion $E(\mathbf{k}_\parallel)$ of the surface states is extended to larger $\mathbf{k}_\parallel$. The dispersion is discussed in Sec. III after a description of the experimental procedures in Sec. II. In Sec. IV spin-resolved target-current spectra (TCS) of the upper gap edge at $\bar{\Gamma}$ (X_1 point) are presented. They demonstrate the theoretically predicted[23,24] exchange splitting of a highly excited state at a critical point of the Ni bulk band

structure. The surface-state exchange splittings observed in spin-resolved IPE spectra are compared with a theoretical estimate using the multiple-reflection model. In Sec. V we summarize our conclusions.

II. EXPERIMENT

The experimental setup[25,26] used in the present work is shown schematically in Fig. 1. Spin-polarized photoelectrons are excited in GaAs(001) by means of circularly polarized laser light.[27] A negative-affinity photocathode is obtained by adsorption of Cs and O_2. After electrostatic deflection by 90° a transversely polarized electron beam is directed at the ferromagnetic sample by a transfer optics. The latter is necessary since both the GaAs electron source and the sample are contained in separate vacuum chambers for their independent preparation. The electron-beam parameters were measured with a Faraday cup which was installed in addition to the sample. The divergence of the electron beam was below 2° at a full width at half maximum (FWHM) of 3 mm. The energy distribution of the beam was controlled by operating the Faraday cup as a simple retarding-field analyzer. The energy resolution of this arrangement is impeded by the inhomogeneity of the deceleration field between the Faraday cup and the grounded last lens element of the transfer optics. Hence the FWHM of 350 meV (at cathode emission currents of typically 5 μA), obtained from the retarding-field current characteristics by numerical differentiation, must be regarded as an upper bound.

The single-crystal Ni sample had the shape of a square picture frame with all legs parallel to a $\langle 110 \rangle$ axis. The legs had a cross section of 3×3.5 mm^2 and an outer length of 13.5 mm. An uncovered self-supporting ten-turn magnetization coil was wound around one leg. The magnetization of nickel crystals is very sensitive to stress, and so massive electric contacts must be avoided. The sample was therefore heated by electron bombardment instead of direct "Ohmic" heating. For preparation and characterization of the sample conventional sputter facilities, low-energy electron diffraction (LEED), and Auger electron spectroscopy were employed.

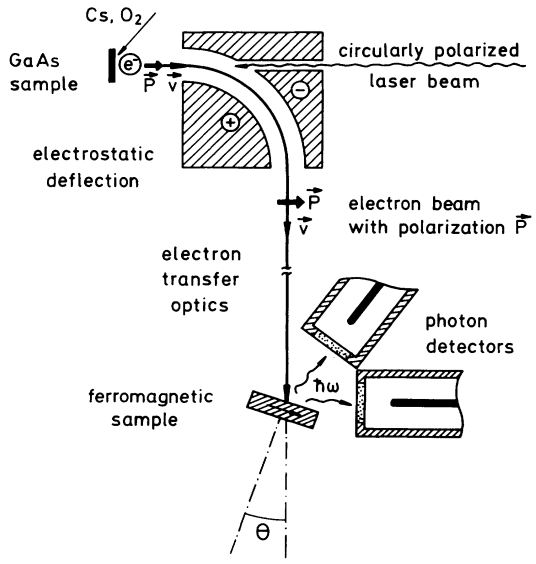

FIG. 1. Schematic of the spin-resolved IPE apparatus.

The Ni(001) crystal was mounted in such a way that the angle of electron incidence could be varied in the ΓXUL mirror plane by rotating the sample. Photons emitted by the sample are simultaneously collected by two iodine bandpass counters placed at different angles in the mirror plane (Fig. 1). The bandpass characteristics of the counters is due to the combined action of the I_2 excitation threshold for molecular photoionization and the transmission cutoff of a SrF_2 entrance window. The photon detection energy centers at 9.43 eV and has a variance of $\sigma^2_{\text{opt}} = (113 \pm 8 \text{ meV})^2$.[28] The use of two counters at different photon detection angles allows one to analyze the angular distribution of radiative transitions and hence the parity of the final states involved in the transition.[8]

Both the energy distribution of the primary electron beam and the optical resolution contribute to the overall energy resolution of the apparatus. The corresponding variance σ^2_{expt} is given in these terms by

$$\sigma^2_{\text{expt}} = \sigma^2_{\text{electron}} + \sigma^2_{\text{opt}} , \tag{1}$$

since variances are additive upon convolution. The variance $\sigma^2_{\text{expt}} = (167 \pm 7 \text{ meV})^2$ was derived directly from the spectral linewidth of the image-potential surface state at $\bar{\Gamma}$ (Sec. IV C) since the intrinsic linewidth of the states[29,30] is one order of magnitude smaller. By means of Eq. (1) a FWHM of 285 ± 30 meV is obtained for the electron energy distribution independently of the retarding-field measurement if we assume a Gaussian line shape. (The FWHM of a Gaussian function is related to the variance σ^2 by FWHM $= 2\sigma\sqrt{2 \ln 2}$.)

For unique detection of spin asymmetries it is necessary to exclude any artificial "asymmetries" resulting from the apparatus. An important operational check is based on the fact that spin effects only depend on the *relative* orientation of the electron-beam polarization and quantization axis, i.e., the sample magnetization. A "true" spin effect in the spectra should remain unaffected upon *simultaneous* reversal of both polarization and magnetization, but should change sign upon reversal of only one vector. In all spin-resolved measurements one series of spectra was recorded for each of the four possible combinations. The spin asymmetries and hence the resulting spin splittings were—except for the sign—identical within counting statistics. The highest insensitivity to long-term drifts of the apparatus was obtained by measuring the spin-resolved spectra *quasisimultaneously:* For each spectral energy the electron-beam polarization was reversed after a few seconds by switching the helicity of the light on the GaAs photocathode through a Pockels cell.

The light transmitted by the transverse Pockels cell was observed to contain a nonvanishing fraction of *linearly* polarized light which varies in time and amounts to 10% in intensity. This nonideal behavior was found for all three of the different cells tested within this work and is presumably characteristic of many cells. The theoretical electron spin polarization of 50% for the GaAs source[27] is not achieved in experiments. This fact

has been attributed to depolarization effects of the electrons in the $Cs\text{-}O_2$ adlayer but can be partly due to incomplete circular polarization of the incident light: At a fraction of 10% linearly polarized light not more than 45% spin polarization can be expected theoretically. In previous experiments with a stable Pockels cell providing circularly polarized light with only a small fraction of linear polarization (maximum up to 2%), a spin polarization of $(33\pm3)\%$ was reproducibly obtained,[26] irrespective of the aging of the photocathode. In specifying the uncertainty in the spin-splitting values determined in this work, we have taken into account any reduction of the source polarization that may occur as a result of the nonideal behavior of the Pockels cells used here.

With aging, the work function of the cathode changed by about 100 meV within a continuous operating time of 150 h. This leads to a corresponding shift of the onset energy in the IPE spectra. Work-function changes of 20 meV can safely be detected and were compensated by an offset to the acceleration voltage. This allowed the entire aging time of the cathode to be used for the accumulation of spectra in order to improve statistics.

For measurement of energy dispersion relations the parallel momentum of the incoming electrons, i.e., their angle of incidence θ on the sample, must be known as precisely as possible. On Ni(001) normal incidence can be determined by means of the intense IPE *sp*-band bulk transition since the photon-counting rate at the low-energy side of the transition reveals a sharp maximum at $\theta=0°$ (Fig. 2). To minimize the influence of magnetic fields on the low-energy electron beam the vacuum chamber was equipped with a Co-Netic^{TM} liner and the vertical component of the Earth's magnetic field was compensated by a pair of Helmholtz coils. The residual field at the position of the sample was below 10^{-7} T. In addition, only truly nonmagnetic materials were used in the vicinity of the electron beam. An independent alternative for calibration of the angle θ is to measure the angular dependence of the current absorbed by the sample.[31] At any constant beam energy the absorbed current must be symmetric with respect to $\theta=0°$ because of the fourfold symmetry of the Ni(001) surface. Hence this

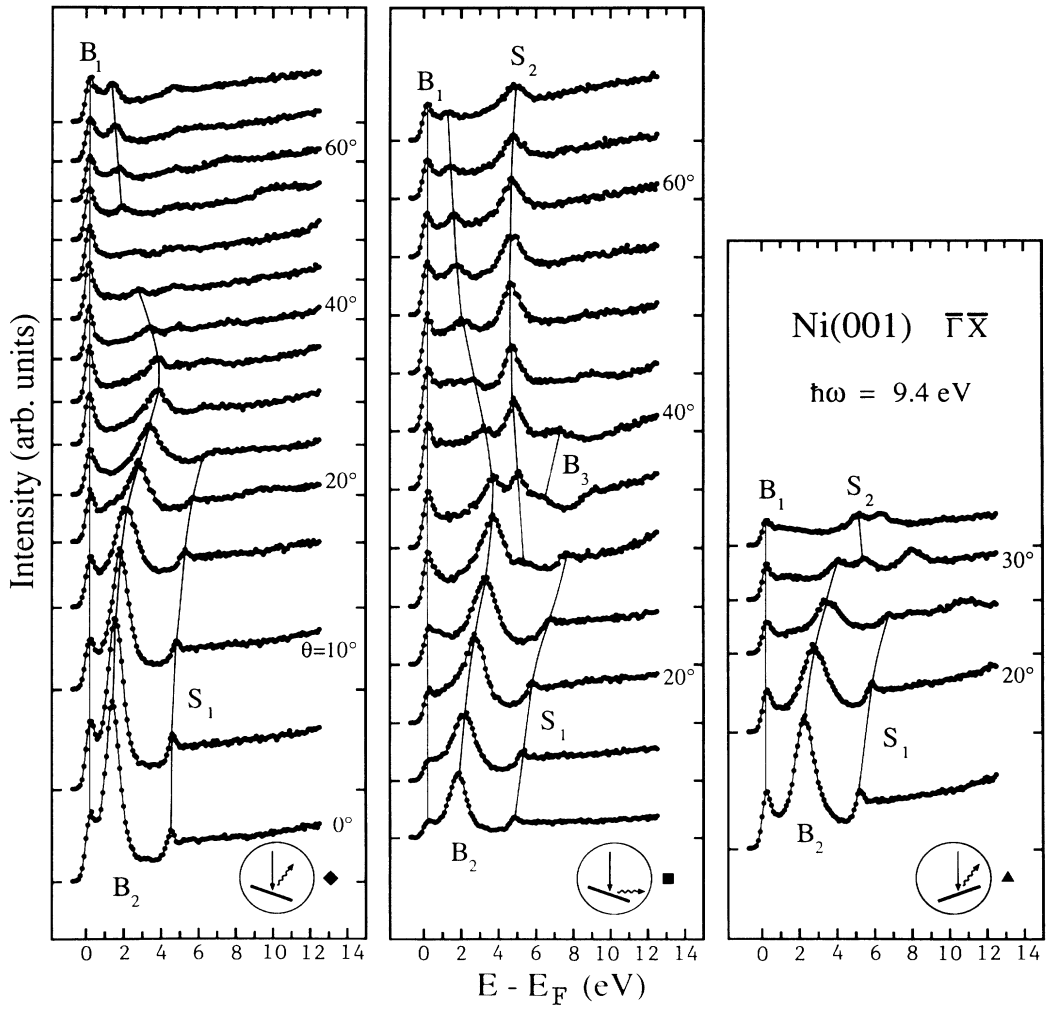

FIG. 2. Angle-resolved IPE spectra of Ni(001) of the ΓXUL mirror plane for different photon-detection geometries indicated at the lower right of each panel.

method allows a check of a possible influence of residual magnetic stray fields on the electron beam at any angle θ. The two methods lead to the same calibration for normal incidence (with $\pm 1°$ accuracy). Reversing the sample magnetization had no effect on the electron beam.

Any spin asymmetry obtained experimentally is dependent on the inner product $\mathbf{P}\cdot\mathbf{J}$ between the electron-beam polarization $\mathbf{P}$ and the average sample magnetization $\mathbf{J}$.[32] The spin-resolved spectra refer to the case of $\mathbf{P}\cdot\mathbf{J}=J$, which is equivalent to a hypothetical polarization of the incident electron beam of 100% and $\mathbf{P}\|\mathbf{J}$. The count rates $N_\uparrow$ ($N_\downarrow$) expected in this case for electrons with spin parallel (antiparallel) to $\mathbf{J}$ are calculated from the count rates $n_{\uparrow,\downarrow}$ (raw data) obtained with the experimental polarization P using

$$N_{\uparrow,\downarrow}=\frac{n_\uparrow+n_\downarrow}{2}(1\pm A)\ , \tag{2}$$

with the spin asymmetry defined as

$$A=\frac{n_\uparrow-n_\downarrow}{n_\uparrow+n_\downarrow}\frac{1}{P}\frac{1}{\cos\theta}\ . \tag{3}$$

θ denotes the angle of electron incidence. The average magnetization $\mathbf{J}$ seen by the low-energy electron beam is mainly determined by the structure of the Weiss domains at the surface. Let the sample be in a single domain state with $\mathbf{J}$ parallel to the long axis of the crystal leg $\langle 110\rangle$. Then the angle of electron incidence θ is identical to the angle between $\mathbf{P}$ and $\mathbf{J}$ and hence the spin-revolved spectra $N_\uparrow$ ($N_\downarrow$) are directly comparable with theoretical band structures. [The latter are calculated for the case of electrons with spin parallel (antiparallel) to the quantization axis.] In the case of any other domain structure the angle between $\mathbf{P}$ and the average magnetization $\mathbf{J}$ is larger than θ in Eq. (2). [This is strictly valid for normal incidence. At off-normal incidence the assumption of a vanishing average magnetization component normal to the surface is necessary. The validity of this assumption is expected for a magnetically soft material such as Ni (Ref. 33) and was checked *in situ* by polar magneto-optical Kerr-effect (MOKE) measurements.]

Throughout the present work we applied Eqs. (1) and (2) without regard for the "true" surface domain structure. The factor $1/\cos\theta$ in Eq. (2) is smaller than or equal to a factor for the true structure. The asymmetry A and any spin splitting obtained from the spectra $N_{\uparrow,\downarrow}$ are therefore *lower bounds* regarding the influence of the complex domain structure expected for the Ni(001) surface.

Owing to the magnetocrystalline anisotropy, Weiss domains in Ni are magnetized along $\langle 111\rangle$, the axes of easy bulk magnetization at room temperature. Ni(001) does not contain an easy axis so that a complex structure of (flux) closure domains is generally found at the surface.[34] It will be demonstrated elsewhere[20] that on surfaces without an easy axis closure domains can lead to a drastic *reduction of the average surface magnetization* in the remanent state and thereby hinder the detection of spin effects. Thus in spin-resolved measurements at surfaces such as Ni(001) the identification of spin effects affords a "magnetic preparation" in addition to the usual preparation of atomically clean and well-ordered surfaces.

The magnetic preparation used for Ni(001) is based on the fact that the crystalline anistropy energy in Ni rapidly decreases with increasing temperature.[35] The sample was heated to 540 K, where the magnetization (in the central region of a leg) could be homogeneously oriented in small external fields (order of 1 $\mathrm{A\,cm^{-1}}$). At *remanence* this single-domain state is stabilized by friction of domain-wall motion and persisted almost completely as the sample cooled down to 340 K during measurement. In this temperature interval closure domains led to a reduction of the average surface magnetization by only 10% as compared with saturation.[20] This procedure yields a much higher average magnetization than was achieved in the IPE investigation of Ni(001) by Klebanoff *et al.*[18]

III. ENERGY DISPERSION

Momentum-resolved IPE spectra in the $\bar{\Gamma}\bar{X}$ azimuth of Ni(001) between 0 and 12 eV above the Fermi energy E_F are shown in Fig. 2. The observed transitions are displayed in the form of an $E(\mathbf{k}_\parallel)$ diagram in Fig. 3. The angle of electron incidence was varied between normal incidence and 70° off normal, the range being extended as compared with the previous IPE study of low-index Ni

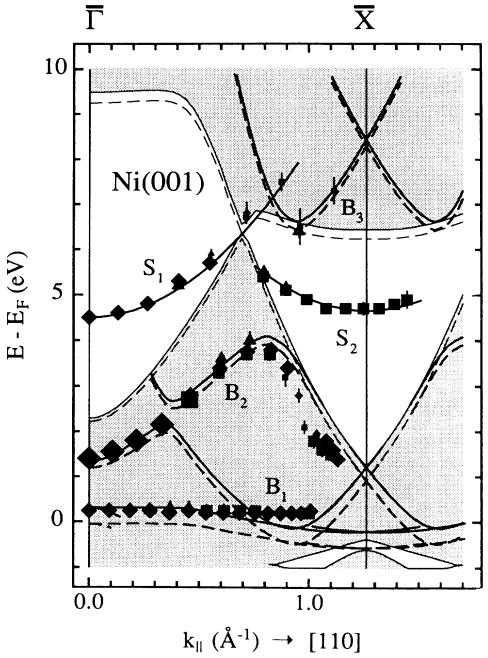

FIG. 3. $E(k_\parallel)$ diagram of the IPE transitions at $\hbar\omega=9.4$ eV on Ni(001) in the $\bar{\Gamma}\bar{X}$ azimuth. Solid (dashed) lines show transitions into minority (majority) states which are kinematically allowed according to a combined-interpolation-scheme calculation. White areas within solid (dashed) borderlines denote the gaps of the projected minority (majority) bulk band structure. Different photon-detection geometries are indicated by the same symbols as in Fig. 2.

surfaces by Goldmann *et al.*[15] Furthermore, in the present work photons were collected at different angles by using separate counters. The photon detection angles are indicated schematically in each of the three panels (bottom) of Fig. 2. These different detection geometries are reflected by different symbols in Fig. 3; their size indicates the observed transition intensities. For comparison, theoretically expected bulk transitions from a combined-interpolation scheme band structure[36] are included; the data were kindly supplied by Fauster and are based on the high-symmetry points of the theoretical $E(\mathbf{k})$ relation by Eckardt and Fritsche.[23] Heavy solid (dashed) lines show kinematically allowed transitions with $\hbar\omega = 9.4$ eV into minority (majority) states. Energy dispersion and spin dependence of the bulk transitions will be discussed elsewhere.[20,37]

When projected on the (001) surface the Shockley-inverted band gap at the X point of the Ni bulk Brillouin zone—the $X_{4'}$-X_1 gap—appears at $\bar{\Gamma}$, whereas the $L_{2'}$-L_1 gaps leads to the gap at $\bar{X}$ (unshaded areas in Fig. 3). The surface state S_1 in the bandgap at $\bar{\Gamma}$ has been previously identified[15] as an image-potential state. At $\bar{\Gamma}$ it is observed as a clear peak at 4.5 eV above E_F; with the Ni(001) vacuum energy of 5.3 eV (Ref. 38) this gives a binding energy of about 0.8 eV. S_1 shows the expected free-electron-like dispersion with an effective mass $m^*/m = (0.95 \pm 0.15)$ for $k_\parallel \leq 0.55$ Å^{-1}. The state S_2 in the gap at $\bar{X}$ is a crystal-induced surface state. In earlier IPE studies with angle-integrated photon detection S_2 only appeared as a weak shoulder.[15] In the present work S_2 is observed as an intense peak through the photon counter placed nearly normal to the surface but with almost vanishing intensity through the other counter (Fig. 3). The dipole axis of the transition is therefore approximately normal to the surface and consequently S_2 has even parity with respect to the ΓXUL mirror plane (Sec. IV). The improved signal-to-background ratio, by means of the second counter, allows the dispersion of the crystal-induced state to be traced even beyond the SBZ boundary. As in the case of Cu(001),[39,40] the upward dispersion is a consequence of the $k_\parallel$ dependence of the gap edges.[41]

The dispersion of bulk and surface states on Ni(001) in Fig. 2 is in accord with general trends observed in recent work on other fcc (001) surfaces.[40,42] But for larger angles of incidence it differs systematically from the Ni(001) data by Goldmann *et al.*[15] In the present work only nonmagnetic materials were employed for the sample holder and in the vicinity of the electron beam. Furthermore, in contrast to earlier measurements magnetic stray fields from the sample itself are minimized by the closed-flux geometry of the picture-frame crystal. Possible residual fields were so small that reversing the sample magnetization had no effect on the electron beam. (Sec. II). It is thus conjectured that magnetic stray fields led to erroneous calibration for the angle of electron incidence in the earlier experiments.

IV. EXCHANGE SPLITTING

The top atomic layer of metal surfaces and the bulk underneath have different electronic structures. Hence their magnetic properties such as exchange coupling and magnetization can be different as well. For Ni(001) Landolt and Campagna[4] showed by polarization analysis of field-emitted electrons that the spin-resolved densities of states of surface and bulk are very similar at the Fermi energy E_F. This allowed them to exclude magnetically "dead" surface layers. This result was corroborated by electron-capture spectroscopy (ECS).[6] Using spin-polarized LEED, Feder *et al.*[6] found the magnetization of the first atomic layer on Ni(001) to be slightly enhanced by $(5 \pm 5)\%$ as compared with the bulk. An enhancement of 20%, as expected from self-consistent local-spin-density-functional calculations,[9] has not been confirmed by experiment. Altogether it follows that the magnetization in the top layer of Ni(001) is very similar to the magnetization in the layers underneath.

What size of the exchange splittings can be expected for the *sp*-like surface states S_1 and S_2? The wave function of the image-potential state S_1 has its maximum probability a few Å in front of the crystal surface and hence has only a small overlap with bulk electronic bands. The spin dependence of S_1 should therefore also be small. In contrast, the wave function of the crystal-induced state S_2 peaks in the top atomic layer and a much larger spin dependence has to be expected.

A. Theoretical predictions

A quantitative estimate of the exchange splittings of *sp*-like surface states can be obtained in the multiple-reflection model of Echenique and Pendry,[13] McRae,[43] and Smith.[44] Borstel and Thörner[14] employed this model for the case of Fe(110). In the model a bound surface state is regarded as a standing plane wave captured between the crystal and the image-potential surface barrier. The amplitude of the wave changes by $r_C e^{i\Phi_C}$ on each reflection at the crystal and by $r_B e^{i\Phi_B}$ at the barrier. r and Φ denote the relevant reflection coefficients and phase changes, respectively. After an infinite number of reflections the amplitude becomes $(1 - r_C r_B e^{i(\Phi_C + \Phi_B)})^{-1}$. A pole in this expression denotes a bound surface state. It can therefore only exist inside a bulk band gap ($r_C = 1$) and below the vacuum energy E_V ($r_B = 1$) at an energy such that

$$\Phi_C + \Phi_B = 2\pi n \ , \tag{4}$$

where n is an integer. In order to meet this condition at least one of the two phases, Φ_C or Φ_B, should rapidly change with energy; accordingly, the states are formally distinguished as either crystal-induced or image-potential states.[13]

The barrier potential and hence Φ_B are assumed to be spin independent.[14] Using this approximation the exchange splitting of *sp*-like surface states is a consequence only of the *spin-dependent* energy position of the *band-gap boundaries.*

The exchange splitting of a Shockley-inverted gap is, in principle, larger at the upper than at the lower edge: While the upper *s*-like states can hybridize with the "magnetic" 3*d* states, such hybridization is symmetry-

forbidden for the lower *p*-like states at the high-symmetry points Γ, X, and L. In effective one-particle Ni band-structure calculations Eckardt and Fritsche[23] and Noffke[24] found a large contribution of *d*-like states at the critical points X_1 and L_1 and thus predicted considerable exchange splittings for the upper edge of the two gaps on Ni(001): 200 meV at $\bar{\Gamma}$ and 230 meV at $\bar{X}$.

The multiple-reflection model is adopted here for the purpose of obtaining an estimate, and approximations are used for the energy dependence of the phases.[45] The energy dependence of the crystal phase Φ_C is described in the two-band model,[41] and it is assumed that Φ_C changes by π on traversing the gap despite the nearby *d* bands.[46] The barrier phase is approximated by McRae's formula.[43] Figure 4 shows the spin-dependent crystal phases along with the associate barrier phases for $\bar{\Gamma}$ (left) and $\bar{X}$ (right). The *absolute* energy position of the states, as given by the intersection of Φ_B with $2\pi n - \Phi_C$ [Eq. (4)], depends on the parameters chosen (e.g., position of image plane). But the *energy difference* of the spin-dependent intersections (splitting) does not critically depend on these parameters, so that for the estimate intended here it is not necessary to adapt the absolute energies to the experimental values.

For the image-potential state ($n=1$) at $\bar{\Gamma}$ only a very small exchange splitting of 10–20 meV can be expected. This is because of the slow energy variation of Φ_B in the vicinity of the $n=1$ intersections. For the crystal-induced state at the SBZ boundary the situation is completely different: At $\bar{X}$ the effective vacuum energy $E_V+\hbar^2\mathbf{k}_\parallel^2/2m$ lies more than 11 eV above E_F so that Φ_B traverses the gap nearly vertically. Thus the exchange splitting of the crystal-induced state has almost the same size as the splittings of the gap boundaries. For S_2 we expect a splitting of about 200 meV.

This simple estimate is in accord with a Ni(001) slab calculation by Wimmer, Freeman, and Krakauer.[9] They predict an even-parity surface state in the gap at $\bar{X}$ at about 5 eV above E_F. It should be exchange split by about 0.25 eV. From symmetry and energy position the theoretically predicted state can be identified with S_2 (Sec. III).

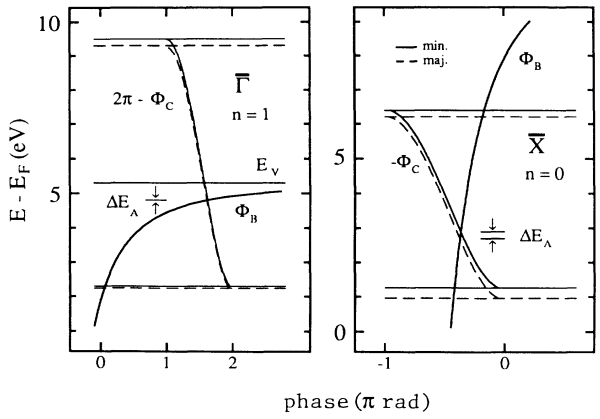

FIG. 4. Estimate of the exchange splitting of *sp*-like surface states on Ni(001) using the multiple-reflection model. The energy values of the minority band gaps are obtained by a combined-interpolation-scheme calculation based on the critical point energies by Eckardt and Fritsche (Ref. 23).

B. Spin dependence of absorbed current

The spin dependence of the electron current absorbed by ferromagnetic surfaces was first investigated by Siegmann, Pierce, and Celotta.[47] Spin-resolved target-current spectroscopy (TCS) has so far only been applied to Fe(001).[48,49] For normal electron incidence on that surface ($\bar{\Gamma}$) the spin asymmetry of the absorbed current reveals a peaked structure with a maximum asymmetry of 7% at 11 eV above the vacuum energy E_V. Since exchange splittings in Ni are roughly one order of magnitude smaller, spin effects in the TCS spectra of Ni surfaces are expected to be smaller as well.

Figure 5(a) shows the spin-resolved absorbed current on Ni(001) $\bar{\Gamma}$ between 0 and 8 eV above E_V. E_V is 5.3 eV (Ref. 38) above E_F. At $\bar{\Gamma}$ (Γ-X direction) the incoming electrons can couple to bulk bands with Δ symmetry which span the $X_{4'}$-X_1 gap . At about 4 eV above E_V the target current curves clearly increase but remain structureless and flat at higher energies (up to at least 40 eV). The increase of the absorbed current occurs between 9 and 10 eV with reference to E_F, i.e., at the upper edge of the $X_{4'}$-X_1 gap (Fig. 3). The energy of steepest ascent is different for majority and minority electrons. This is clearly revealed by the first derivatives of the target-current curves in Fig. 5(b): The maxima are split by (230±70) meV. The error is dominated by the uncertainties of the background in the TCS asymmetry (see below) and the electron-beam polarization. The derivative spectra are obtained by convoluting the target-current curves in Fig. 5(a) by the first derivative of a Gaussian function with a variance of (50 meV)^2.[28]

The energy of steepest ascent (turning point) in the target-current curves is not identical with the energy position of X_1, since the group velocity of the Δ bands vanishes at the critical point.[50] Hence an incoming electron can only couple to the bulk bands at energies above X_1. The exact energy position of the turning point also depends on the band dispersion.[51] In first approximation the dispersions of the spin-dependent Δ bands near X_1 differ only by a constant, which is the exchange splitting

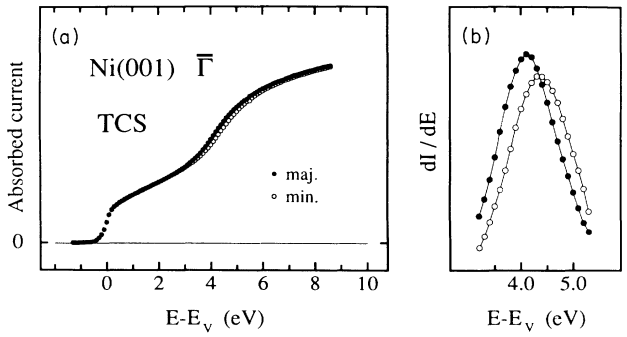

FIG. 5. Spin-resolved absorbed current on Ni(001) $\bar{\Gamma}$ (a) and exchange splitting at the critical point X_1 (b). (For explanations see the text.)

at X_1. The spin splitting of the turning points thus *directly* gives the exchange splitting at X_1. As for all experimental values for spin asymmetries and splitting given in this work, the value of 230 meV is a lower bound with respect to the influence of closure domains (Sec. II).

The spin asymmetry associated with the target-current curves is presented in Fig. 6 (solid dots). Because of the exchange splitting the absorption of majority electrons dominates at X_1, which gives rise to a pronounced peak with a maximum of 3% at 4.1 eV above E_V. Although this TCS spin asymmetry is small, it can in principle be precisely detected with little effort. In practice, the accuracy of detection was limited by the quality of the electron beam. The open squares in Fig. 6 give an example of the TCS spin asymmetry with different lens parameters of the electron transfer optics: The two asymmetry curves show a different background. Owing to minor deflections of the laser beam in the Pockels cell when switching the helicity, the middle axis of the electron beam was not exactly identical for the two polarization directions, as was proved by measurement of the beam's vertical cross section with a Faraday cup. Since the FWHM of the beam was not much smaller than the sample width, the primary electron current on the sample changed by up to 1% when switching the polarization. This small difference has no effect on the IPE spectra discussed below, since they are normalized to a preset charge absorbed by the sample. But such small effects must in general be considered in the discussion of spin-revolved TCS spectra; here they lead to an uncertainty of about $\frac{1}{5}$ in determining the asymmetry in the peak maximum in Fig. 6.

In the current *reflected* from Fe(001) Tillmann, Thiel, and Kisker[49] observed a large spin asymmetry of 21% which they suggested be used as a polarization detector. When different detectors are being compared, the quantity $A^2 I/I_0$ serves as a figure of merit[32] since for efficient polarization measurement a large fraction I/I_0 of the primary electron beam I_0 must be analyzed in a process with high asymmetry A. The achievable figure of merit is 3.5×10^{-3} for Fe(001) as compared with "only" a few times 10^{-4} in the case of Ni(001), investigated here. However, this value is respectable in comparison with the figure of merit of 2.3×10^{-4} (Ref. 52) achieved in conventional detectors based on Mott scattering. For a practical use of the Ni(001) spin asymmetry the sample must be held at elevated temperatures since at room temperature closure domains usually lead to a reduction of the average surface magnetization.[19,20]

The observed exchange splitting of (230±70) meV at the X_1 point is in reasonable agreement with the theoretical prediction of 200 meV.[24] This demonstrates the existence of strong hybridization of a highly excited free-electron-like band about 10 eV above E_F with the Ni $3d$ bands. In estimating the exchange splitting of the surface states we assumed splittings of the order of 200 meV for the upper gap edges. In the case of the X_1 point this assumption is now justified by experimental data.

C. Surface states

In Fig. 7 spin-resolved IPE spectra of the image-potential state S_1 at $\bar{\Gamma}$ are presented along with the associated spin asymmetry. The background in the IPE spectra is also spin polarized, as already mentioned.[53,8] Hence, although the asymmetry reveals a significant structure at the position of the two peaks, such a structure must be regarded with caution. It does not necessarily indicate energy splitting of the peaks, since even nonsplit peaks on a polarized background result in a decrease of the spin asymmetry in the peak region. This is evident from Eq. (3): Nonsplit peaks are an unpolarized contribution to the count rates $n_{\uparrow,\downarrow}$, which only leads to an increase of the denominator.

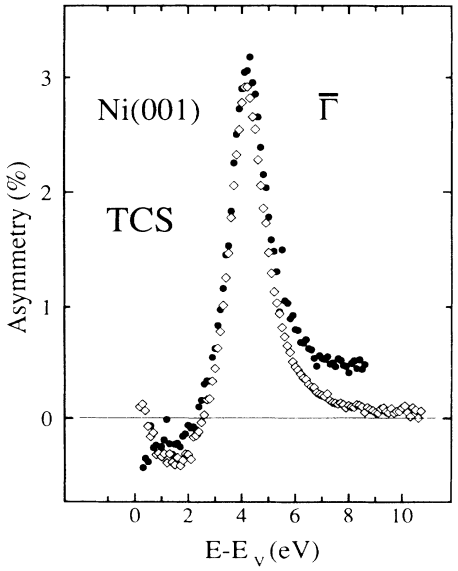

FIG. 6. Spin asymmetry of the absorbed current on Ni(001) $\bar{\Gamma}$.

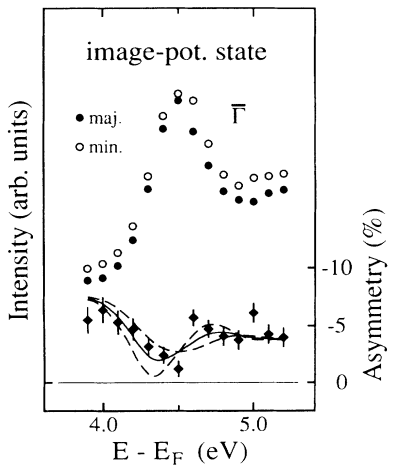

FIG. 7. Spin-resolved IPE spectra of the Ni(001) image-potential state ($n=1$) at $\bar{\Gamma}$ ($\hbar\omega=9.4$ eV) with the associate spin asymmetry (diamonds). Solid and dashed lines show hypothetical asymmetries which refer to different sizes of the exchange splitting.

In order to identify possible spin splitting, the peak positions in the spin-resolved spectra were determined by least-squares fits. In IPE spectra the line shape and background form—both necessary for characterizing the spectra in the fitting procedure—are not known *a priori*.

The intrinsic linewidth of image-potential states is of the order of several times 10 meV (Refs. 29 and 30) and is thus much smaller than our overall resolution of about 400 meV FWHM. A Gaussian line shape (instrumental response function) was therefore assumed for the peaks. In the case of the spectra in Fig. 7 the absolute peak position of the lines as determined by the fit depends on the function chosen to describe the background. The peak position of the lines determined by the fit is changed, e.g., by more than 20 meV when a purely linear background is assumed instead of a linear background combined with an integrated Gaussian, representing the steplike increase of the background at the peak (see also Fig. 2). This uncertainty in the absolute peak position is even larger than the expected splitting of 10–20 meV (see above). However, the relative energy position of the spin-revolved peaks can be determined with a smaller error if the assumption of a spin-independent background form is made. In the fitting procedure the same functional form is thus used for the background description in the two spectra. The relative energy position of the peaks is found to be almost independent of the four different background functions employed: linear, quadratic, linear plus integrated Gaussian, and linear with a second peak at a fixed energy difference of about 0.64 eV above the image-potential state ($n=1$) in view of a possible contribution from the neighboring ($n=2$) Rydberg state [$E_n=(1\ \mathrm{Ry})/16n^2$]. The smallest and largest values for the energy difference were 10 meV (linear background) and 13 meV (linear plus integrated Gaussian background). The χ^2 values for all fits are well above unity, which can be understood as a consequence of the small number of data points (14 per spectrum): a statistical aberration of a single point leads to a considerable increase of χ^2. The lowest $\chi^2=6.5$ is obtained for the linear plus "integral" background. For this background the confidence interval of the energy difference is [0,26] meV; the confidence intervals which correspond to the other background forms are located within the above interval. The uncertainty of the electron-beam polarization (Sec. II) leads to a negligible contribution (<3 meV) to the experimental error. Consequently, under the above assumption of a spin-independent background form, there is an 83% probability that the image-potential state is exchange split with the most probable value being 13 meV.

In order to check the above result by an analysis which requires no separation of the spectra into line and background, we compare the experimental spin asymmetry with a hypothetical one. The latter is obtained by taking the spin-integrated spectrum as "majority" and—after addition of an offset B and a shift by an energy S—as "minority." It is thus assumed that the line shape is spin independent and that the background only differs by an offset within the spectral region. The experimental asymmetry is described best ($\chi^2=2.3$) when a "splitting" of $S=10$ meV (with an offset $B=-7.5\%$) is assumed. The corresponding hypothetical asymmetry is shown as a solid line in Fig. 7. For comparison, similar curves for $S=0$ (flat curve, $\chi^2=3.1$) and for $S=20$ meV ($\chi^2=3.3$) are included as dashed lines. Although the χ^2 minimum for $S=10$ meV is well above unity, the result supports the value obtained by the fitting procedure.

Figure 8 shows spin-resolved spectra of the crystal-induced state S_2 at $\theta=50°$ near $\bar{X}$ (corresponding to $\theta=56°$). The majority and the minority peak are clearly spin split. The size of the splitting is (180 ± 60) meV, as determined by least-squares fits in which a linear background (see Fig. 2) with spin-dependent slopes was assumed. The main contribution (50 meV) to the experimental error is due to the uncertainty of the beam polarization. The splitting of the transition is in a good approximation equal to the exchange splitting of the final state since the energy of S_2 is a stationary function of $\mathbf{k}_\parallel$ at $\bar{X}$.

Close inspection of the spectra in Fig. 8 shows that the width of the minority line is about 10% larger than that of the majority line. So far a shorter lifetime of unoccupied minority states has only been observed in bulk transitions,[8] where it seems plausible because of the unoccupied density of states at E_F being larger for minority electrons.[54] The wave function of a crystal-induced state has considerable overlap with bulk bands into which the surface state can decay. A spin-dependent lifetime of the crystal-induced state S_2 therefore seems reasonable.

The exchange splitting of both the image-potential state S_1 and the crystal-induced state S_2 is of the size expected from the estimate. The large splitting of S_2 is a consequence of the exchange splitting of the free-electron-like bands at the upper gap boundary, here at the L_1 point. We propose the same explanation for the splitting of the crystal-induced state in the $X_{4'}$-X_1 bandgap on Ni(110).[8] Furthermore, the large splitting of the crystal-induced state demonstrates *directly* that the top atomic layer of Ni(001) is magnetically active.

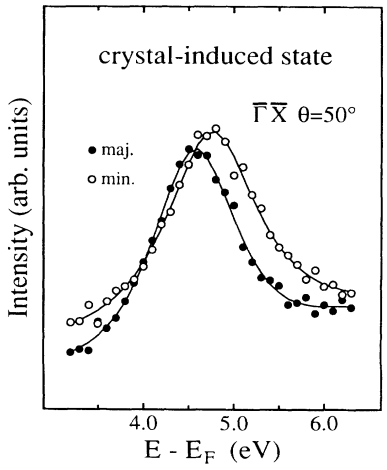

FIG. 8. Spin-resolved IPE spectra of the Ni(001) crystal-induced state ($n=0$) near $\bar{X}$ ($\hbar\omega=9.4$ eV).

V. SUMMARY AND CONCLUSION

For a highly excited state at the upper boundary of a Shockley-inverted gap a large exchange splitting is observed by spin-revolved TCS. This result demonstrates the theoretically predicted strong hybridization of free-electron-like bands with 3*d* bands even several eV above the Fermi energy. The spin splitting of both types of *sp*-like surface states on Ni(001) is determined by spin-resolved IPE. The comparison between experiment and an estimate using the multiple-reflection model shows that the exchange splittings of the crystal-induced and the image-potential Ni surface states, although widely different in size, can be understood as a consequence of the spin-dependent band-gap boundaries.

The large splitting of the crystal-induced state [(180±60) meV] *directly* demonstrates that the top atomic layer of Ni(001) is magnetically active. There is experimental evidence of nonvanishing exchange splitting of the Ni(001) image-potential state [(13±13) meV]. Work on improving the overall experimental resolution to reduce the detection limit is now in progress.

ACKNOWLEDGMENTS

We are indebted to G. Nagleder for his excellent technical support. Helpful discussions with M. Donath, J. Noffke, and Th. Fauster are gratefully acknowledged.

*Present address: Institut für Experimentalphysik, Freie Universität Berlin, Arnimallee 14, D-1000 Berlin 33, Germany.

[1]L. Liebermann, J. Clinton, D. M. Edwards, and J. Mathon, Phys. Rev. Lett. **25**, 232 (1970).
[2]D. T. Pierce and H. C. Siegmann, Phys. Rev. B **9**, 4035 (1974).
[3]L. Bergmann, Phys. Rev. Lett. **41**, 264 (1978).
[4]M. Landolt and M. Campagna, Phys. Rev. Lett. **38**, 663 (1977).
[5]C. Rau, Comments Solid State Phys. **9**, 177 (1980).
[6]R. Feder, S. F. Alvarado, E. Tamura, and E. Kisker, Surf. Sci. **127**, 83 (1983).
[7]W. Eberhardt, E. W. Plummer, K. Horn, and J. Erskine, Phys. Rev. Lett. **45**, 273 (1980).
[8]M. Donath, V. Dose, K. Ertl, and U. Kolac, Phys. Rev. B **41**, 5509 (1990).
[9]E. Wimmer, A. J. Freeman, and H. Krakauer, Phys. Rev. B **30**, 3113 (1984).
[10]A. Goldmann, V. Dose, and G. Borstel, Phys. Rev. B **32**, 1971 (1985).
[11]F. J. Himpsel, Adv. Phys. **32**, 1 (1983).
[12]R. Courths and S. Hüfner, Phys. Rep. **112**, 53 (1984).
[13]P. M. Echenique and J. B. Pendry, J. Phys. C **11**, 2056 (1978).
[14]G. Borstel and G. Thörner, Surf. Sci. Rep. **8**, 1 (1988).
[15]A. Goldmann, M. Donath, W. Altmann, and V. Dose, Phys. Rev. B **32**, 837 (1985).
[16]K. Giesen, F. Hage, F. J. Himpsel, H. J. Riess, W. Steinmann, and N. V. Smith, Phys. Rev. B **35**, 975 (1987).
[17]H. Scheidt, M. Glöbl, V. Dose, and J. Kirschner, Phys. Rev. Lett. **57**, 1688 (1983).
[18]L. E. Klebanoff, R. K. Jones, D. T. Pierce, and R. J. Celotta, Phys. Rev. B **36**, 7849 (1987).
[19]K. Starke, K. Ertl, M. Donath, and V. Dose, Vacuum **41**, 755 (1990).
[20]K. Starke, K. Ertl, and V. Dose (unpublished).
[21]N. Fischer, S. Schuppler, T. Fauster, and W. Steinmann, Phys. Rev. B **42**, 9719 (1990).
[22]F. J. Himpsel, Phys. Rev. B **43**, 13 394 (1991).
[23]H. Eckardt and L. Fritsche, J. Phys. F **17**, 925 (1987).
[24]J. Noffke (private communication).
[25]U. Kolac, M. Donath, H. Liebl, and V. Dose, Rev. Sci. Instrum. **59**, 1933 (1988).
[26]M. Donath, Appl. Phys. A **49**, 351 (1989).
[27]D. T. Pierce and F. Meier, Phys. Rev. B **13**, 5484 (1976).
[28]V. Dose, T. Fauster, and R. Schneider, Appl. Phys. A **40**, 203 (1986).
[29]R. W. Schoenlein, J. G. Fujimoto, G. L. Eesley, and T. W. Capehart, Phys. Rev. Lett. **61**, 2596 (1988).
[30]S. Schuppler, N. Fischer, T. Fauster, and W. Steinmann, Appl. Phys. A **51**, 322 (1990).
[31]R. Schneider, H. Dürr, T. Fauster, and V. Dose, J. Vac. Sci. Technol. A **8**, 3363 (1990).
[32]J. Kessler, *Polarized Electrons* (Springer, Berlin, 1985).
[33]A. Hubert, *Magnetic Domains* (Springer, Berlin, in press)
[34]D. Krause and H. Frey, Z. Phys. **224**, 257 (1969).
[35]M. I. Darby and E. D. Isaac, IEEE Trans Magn. **MAG-10**, 259 (1974).
[36]N. V. Smith and L. F. Mattheiss, Phys. Rev. B **9**, 1341 (1974).
[37]R. Schneider, K. Starke, K. Ertl, M. Donath, V. Dose, J. Braun, M. Grass, and G. Borstel, J. Phys. Condens. Matter (to be published).
[38]K. Wandelt, in *Thin Metal Films and Gas Chemisorption,* edited by P. Wissmann (Elsevier, Amsterdam, 1987).
[39]M. Donath, M. Glöbl, B. Senftinger, and V. Dose, Solid State Commun. **60**, 237 (1986).
[40]R. Schneider, IPP Report No. 9175, Garching: Ph.D. thesis, Universitä Würzburg, 1989.
[41]C. T. Chen and N. V. Smith, Phys. Rev. B **35**, 5407 (1987).
[42]W. Altmann, IPP Report No. 9166, Garching: Ph.D thesis, Universität Würzburg, 1988.
[43]E. G. McRae, Rev. Mod. Phys. **51**, 541 (1979).
[44]N. V. Smith, Rep. Prog. Phys. **51**, 1227 (1988).
[45]In Ref. 22 the splitting of image-potential states at Co(0001)$\bar{\Gamma}$ and Fe(110)$\bar{\Gamma}$ is also estimated by using the multiple-reflection model with the same phase approximations.
[46]J. B. Pendry and S. J. Gurman, Surf. Sci. **49**, 87 (1975).
[47]H. C. Siegmann, D. T. Pierce, and R. J. Celotta, Phys. Rev. Lett. **46**, 452 (1981).
[48]T. Dodt, D. Tillmann, R. Rochow, and E. Kisker, Europhys. Lett. **6**, 375 (1988).
[49]D. Tillmann, R. Thiel, and E. Kisker, Z. Phys. B **77**, 1 (1989).
[50]E. Tamura, R. Feder, J. Krewer, R. E. Kirby, E. Kisker, E. L. Garwin, and F. K. King, Solid State Commun. **55**, 543 (1985).
[51]R. Drube, J. Noffke, R. Schneider, J. Rogozik, and V. Dose, Phys. Rev. B **45**, 4390 (1992).
[52]M. R. Scheinfein, D. T. Pierce, J. Unguris, J. J. McClelland, R. J. Celotta, and M. H. Kelley, Rev. Sci. Instrum. **60**, 1 (1989).
[53]J. Unguris, A. Seiler, R. J. Celotta, D. T. Pierce, P. D. Johnson, and N. V. Smith, Phys. Rev. Lett. **49**, 1047 (1982).
[54]R. Feder and A. Rodriguez, Solid State Commun. **50**, 1033 (1984).

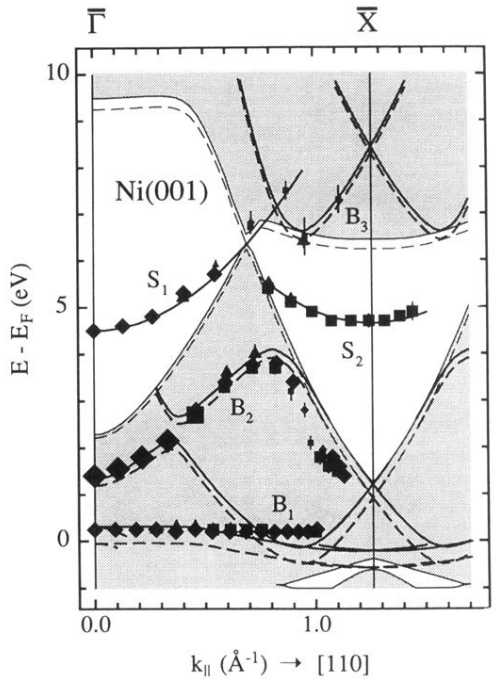

FIG. 3. $E(k_{\|})$ diagram of the IPE transitions at $\hbar\omega = 9.4$ eV on Ni(001) in the $\bar{\Gamma}\,\bar{X}$ azimuth. Solid (dashed) lines show transitions into minority (majority) states which are kinematically allowed according to a combined-interpolation-scheme calculation. White areas within solid (dashed) borderlines denote the gaps of the projected minority (majority) bulk band structure. Different photon-detection geometries are indicated by the same symbols as in Fig. 2.